

Modeling extra-deep EM logs using a deep neural network

Sergey Alyaev, Mostafa Shahriari, David Pardo, Angel Javier Omella, David Selvåg Larsen, Nazanin Jahani, Erich Suter

Abstract

Modern geosteering is heavily dependent on real-time interpretation of deep electromagnetic (EM) measurements. This work presents a deep neural network (DNN) model trained to reproduce the full set of extra-deep real-time EM logs consisting of 22 measurements per logging position. The model is trained in a 1D layered environment and has sensitivity for up to seven layers with different resistivity values. A commercial simulator provided by a tool vendor is utilized to generate a training dataset. The impossibility of parallel execution of the simulator effectively limits the permissible dataset size. Therefore, the geological rules and geosteering specifics supported by the forward model are embraced when designing the dataset. It is then used to produce a fully parallel EM simulator based on a DNN without access to the proprietary information about the EM tool configuration or the original simulator source code. Despite a relatively small training set size, the resulting DNN forward model is quite accurate for synthetic geosteering cases, yet independent of the logging instrument vendor. The observed average evaluation time of 0.15 milliseconds per logging position makes it also suitable for future use as part of evaluation-hungry statistical and/or Monte-Carlo inversion algorithms.

Index Terms

Artificial neural networks, Electromagnetics, Multi-layer neural network, Numerical simulation, Well logging.

I. INTRODUCTION

Recovering sparse hydrocarbon resources requires precise positioning of a well in a subsurface environment burdened by uncertainties. The process of dynamically changing the angle of a well based on measurements acquired and transmitted in real-time from logging while drilling (LWD) tools is commonly called geosteering. The most useful and utilized measurements for geosteering are electromagnetic (EM) measurements, which combine reliability with deep sensitivity (depth of investigation).

Thus, modern geosteering is heavily dependent on real-time interpretation of deep EM measurements [1], [2], [3], [4], . Current generation of Extra-Deep EM tools (also referred to as Ultra-Deep EM) can detect remote boundaries up to 200 ft. away from measurement location [5,], and recent publications have even revealed sensitivity ahead of bit [6,]. The common logging environment for oil or gas saturated reservoirs are high-resistivity reservoir rocks with a capping low-resistive shale on top and a lower-bounding shale or water saturated rocks, both being conductive.

The corresponding real-time interpretation (inversion) requires solution of possibly thousands of forward problems under strict time constraints [7,]. Thus, we need a high computational efficiency, which can be partially achieved by parallel execution. In contrast to simulation software developed in academic environment [8,], many of the existing commercial forward models have limited parallel execution capabilities. Moreover, due to non-disclosed details of proprietary codes, they cannot be easily re-implemented in environments optimized for distributed execution.

To achieve the extreme computational efficiency needed by future geosteering strategies that handle geological uncertainties [9,], we propose a data-based approach using Deep Neural Networks (DNNs) to model the forward problem. The resulting data-based forward solver could be used to invert resistivity measurements using, for example, Bayesian methods. DNNs provide real-time execution of thousands of evaluations, which is essential for complex statistical inversion using, for example, an ensemble Kalman filter [10,] or a Markov Chain Monte-Carlo (MCMC) [11,]. Moreover, approaches based on DNNs are known for extreme efficiency across different hardware architectures, including mobile and embedded options [12,], which paves the way for faster digitalization. Ultimately, one can consider the possibility of running the model on an on-site embedded system.

DNNs [13], [14,] have during the last decade proven their unique ability to overcome essential challenges in various fields of science and technology [15], [16], [17,]. Analogously, the research of DNNs and Machine Learning (ML) techniques have also increased tremendously in the last years in petroleum engineering and computational geophysics [18], [19], [20], [21],

S. Alyaev, N. Jahani and E. Suter are with NORCE, Bergen, Norway

M. Shahriari is with Software Competence Center Hagenberg (SCCH), Hagenberg, Austria

D. Pardo is with the University of the Basque Country (UPV/EHU), the Basque Center for Applied Mathematics (BCAM), and Ikerbasque, Bilbao, Spain
A.J. Omella is with the University of the Basque Country (UPV/EHU)

D.S. Larsen is with Baker Hughes, Stavanger, Norway

© 2020. This manuscript is copyright to the authors and is made available under the license <http://arxiv.org/licenses/nonexclusive-distrib/1.0/>

This version was generated July 4, 2022

Submitted to Geophysics

[22], [23], [24], [25], [26], [27], [28], [29] use a neural network to predict missing dielectric dispersion logs from the available logs. [30] use a multi-layered fully-connected DNN to solve the inversion of resistivity measurements, where the formation is isotropic and the trajectory is constant. [31] consider a more general problem in which the rock properties and the trajectory vary. However, their results exhibit a lack of accuracy in comparison to traditional inversion techniques. This is in part because the inverse problem may have multiple solutions. [32], [33] use a DNN to approximate the forward problem for a 1D medium. Since the forward problem is continuous and has a unique solution, the approximated forward function delivers an acceptable accuracy. The model in [32] is restricted to only three layers. [33] approximates a more complex 2D model with a geological fault, but only considers traditional deep azimuth measurements (above 400 kHz) acquired with shorter spacing instruments.

In this work, we model the full set of extra-deep real-time EM logs consisting of 22 measurements per logging position with a DNN. To take full advantage of the depth of investigation, we train the model to respond to up to 7 layers (three above and three below the logging instrument). For the training (offline) phase, we generate a dataset using a commercial simulator software [34,] that offers no access to the source code. Critical to the success of the proposed methodology is the design of a relatively small application-specific and geologically-consistent training dataset, for which we demonstrate that it yields accurate approximation in the modelled geosteering scenarios.

Thus, we create a scalable EM simulator that is suitable for cluster deployment without having access to neither the source code of the software nor the EM tool configuration. One crucial advantage of the proposed data-driven simulator is its capability of performing over 500 forward evaluations per second during the execution (online) phase. In addition, the resulting DNN software overcomes limitations posed by certain commercial simulators that employ Graphical User Interfaces (GUI), which prevent their massive parallel execution when using MCMC inversion methods.

The article is organised as follows. Section II discusses the forward model and data generation procedures for realistic EM logs. Section III describes our selected deep neural network architecture. The numerical results for the current study are presented in Section IV and the main conclusions are summarised in Section V.

II. FORWARD MODEL AND TRAINING SET GENERATION

We approximate the responses of the Extra Deep EM tool using a DNN. To establish the DNN model, we need a training dataset. In our case, we generate the dataset using a high-fidelity physics-based simulator with a software provided by the tool vendor. [34] describe the vendor's forward EM simulator, which reproduces log responses in a layered medium with arbitrary orientation of layers relative to the tool direction (well angle). In our article, we treat the forward simulator as an unknown function \mathcal{F} . In the following, we describe its inputs and outputs.

A. Model inputs

In our study, we use the inputs native to the simulator with some assumptions to reduce the input space for the sake of training efficiency. We encode a total of seven layers (three above and three below the logging position layer), which is a number often used for practical purposes that is related to the look-around capabilities of the logging instrument. For each layer, the input contains the location of the boundary between layers relative to the measurement point (6 variables, the top and bottom layers are considered to be of infinite thickness) as well as the resistivities parallel and perpendicular to the layer (7×2 variables). Additionally, we encode the local geometry of the well by 2 angles. The first angle is the relative angle between the tool and the downward pointing normal of the layered model. The second angle is the relative angle of the well 20 meters ahead of the receiver. The interpolation between the angles defines the appropriate positions of the tool's transmitters required for the computation.

This parameterization of the local geology around the well, approximated as a layered medium, gives a total of 22 input variables that we denote as vector $\mathbf{P} \in \mathbb{R}^{22}$.

B. Synthetic logs / Model outputs

The model outputs the synthetic logs in the same format as the logging instrument during a drilling operation. Depending on the tool configuration, there can be up to 22 individual measurements utilized for real-time inversion: 4 shallow apparent resistivities and 9 pairs of deep directional measurements. We train the DNN to reproduce all of them. Assuming no azimuth (sideways) angle, we can replace the value-angle pairs of the directional measurements by projecting the directional measurements to the vertical axis yielding one signed number. This gives a total of 13 values in the output, which we denote by $\mathbf{M} \in \mathbb{R}^{13}$.

The logs are grouped in three categories:

- 1) The group of logs denoted RT CRES represent the traditional resistivity logs with a sensitivity up to 5m radial distance from the logging instrument. The measurements are transformed into apparent resistivities with different depth of averaging and are provided in Ohm·m.
- 2) The group denoted RT ARSLLM is an azimuthal resistivity logging instrument operating at 400 kHz. The sampled voltages are processed internally in the tool and provide signal strength and a target direction, which implies the excess

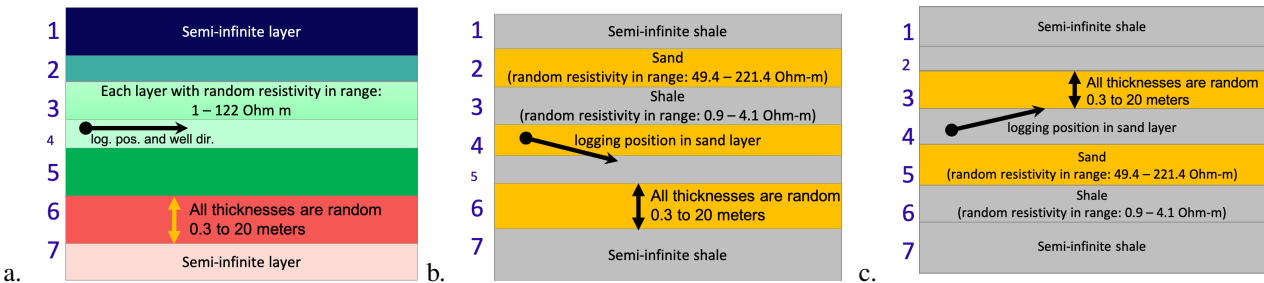


Fig. 1. Schematics of the model inputs' set-ups. The measuring position denoted by a dot with a well direction arrow is located in the middle layer. a. Fully random setup. b-c. Alternating sands and shales: b. Sand as the middle layer. c. Shale as the middle layer.

of conductivity in the EM environment around the transmitter - receiver coil. In a 1D environment, the maximum signal is always oriented in the direction of the layering. Thus, we omit the angle and use the signed value of the signal. The processing provides both real and imaginary components, which are presented in nanovolts (nV). Here we only model the imaginary component which is more useful for geosteering and is provided in real-time.

- 3) The Extra Deep EM tool operates with a frequency of 20 and 50 kHz and deploys a set of synchronized Z receivers and two transmitters, one which is cross oriented for acquiring the azimuthal components [35,]. Its inputs are denoted RT EDAR and RT DTK for azimuthal and non-azimuthal components, respectively. For EDAR the signals are provided in nV and we use the +/- sign to distinguish the maximum signal direction. For DTK the raw signal in decibel (dB) is used.

C. Ground truth data set

The ground truth data set for this study is generated by an automatic workflow. For each input we first select a random realization of inputs according to the rules described below. Then, an AutoIt script [36,] executes the proprietary modeling tool for the selected input models.

For this study, we restrict to the angle range that is most important for geosteering in near-horizontal layering: 80–92 degrees, where 90 degrees means drilling parallel to the layers. We assume that the well trajectory is straight around the measurement point, meaning that no bending in the logging instrument occurs and the transmitters have the same orientation as the receivers. Thus, the two angle parameters are equal. All inner layers in all models have thicknesses uniformly distributed between 0.3 and 20 meters and rounded to 0.1 meters. Also, we restrict to isotropic resistivities for this study.

The initial training dataset containing 22,469 samples consists of a generic layered medium with uniformly distributed resistivities in the logarithmic scale, yielding values between 1 and 122 Ohm·m for each of the layers, see Figure 1a.

Then we enrich the training dataset with 50,492 additional samples containing alternating sand-shale layers that better capture the variety in high contrasts rather than small heterogeneities across the layers. The ability to produce accurate predictions in such high-contrast scenarios is essential and of great value during geosteering operations, so the ML model must be trained with a large number of samples to improve its quality for this specific geological scenario. For that, we consider different sand-shale sequences, where the shales resistivities are in the range 0.9–4.1 Ohm·m, and the sand resistivities are in the range 49.4–221.4 Ohm·m. Within these ranges, resistivities are randomly sampled in the logarithmic scale. We consider two cases with respect to the nature of the middle (logging position) layer. In the case where the logging position is in a sand, see Figure 1b, we generate 25,203 samples with seven alternating layers. In the case where the logging position is in a shale, see Figure 1c, we generate 25,289 samples with five alternating sand-shale layers. Since the sensitivity to the outer-most (1st and 7th) layers is very low, the model is simplified to only 5 layers in this scenario. We implement this by imposing that the two top layers share their electrical properties. The same is imposed on the two bottom layers, see figure 1c.

The total of 72,961 samples comprise what we call the *basic dataset* \mathbf{D}^b .

Early numerical experiments revealed that the dataset dominated by alternating sand-shale layers lacks the data needed to accurately approximate the measurements in thick shale which is typical when approaching a reservoir. Therefore, the dataset is augmented with 11,709 samples of 'semi-degenerate' sand-shale layering. This part of the dataset is generated with the same rules as the high-contrast layers, but for each sample a random number of layers near the top or bottom were assigned the resistivity of the 1st and 7th layer, respectively. The logging position layer always maintains an independent resistivity.

The final *extended dataset*, denoted \mathbf{D}^e , contains 84,599 input-output pairs. We denote the i -th input-output pair (sample) as $(\mathbf{P}_i, \mathbf{M}_i) \in \mathbb{R}^{22} \times \mathbb{R}^{13}$.

The extremely high values of the apparent resistivities near the layer boundaries (often called 'horns') are truncated by the simulator to 2000 Ohm·m. Our experiments indicate that removing such samples from the dataset provides better fit of the final results. The remaining 78,877 samples are split into training (80%), validation (10%), testing (10%) data sets. Testing samples are unused during training, and employed only for quality assessment of the model in subsection IV-B.

III. DEEP LEARNING APPROACH

In this work, we design a DNN-based approximation \mathcal{F}_w (where w stands for finite set of weights) of the forward function \mathcal{F} . In the following, we describe the machine learning algorithm including its rescaling, loss function, architecture, and training process.

A. Rescaling the data

To equalize the effect of each component of the training dataset during the optimization process, we build a min-max linear rescaling over each variable. Note, that for input and output variables representing resistivities we take the logarithm prior to rescaling. We denote these rescaling-functions and their inverses as:

$$\begin{aligned} \Psi_p &:= \{\Psi_p^1, \dots, \Psi_p^p\}, & \Psi_m &:= \{\Psi_m^1, \dots, \Psi_m^m\}, \\ \Psi_p' &: (\mathbb{R}^p) \rightarrow [0.5, 1.5]^p, & \Psi_m' &: (\mathbb{R}^m) \rightarrow [0.5, 1.5]^m, \\ \mathbf{P}_i &= \Psi_p(\mathbf{P}_i), & \mathbf{M}_i' &= \Psi_m(\mathbf{M}_i), \\ \mathbf{P}_i &= \Psi_p^{-1}(\mathbf{P}_i'), & \mathbf{M}_i &= \Psi_m^{-1}(\mathbf{M}_i'), \end{aligned} \quad (1)$$

where p and m are the number of variables (components) in \mathbf{P} and \mathbf{M} , respectively.

The functional approximation of the forward model \mathcal{F}_w consists of the rescaling introduced in (1) and the DNN relation between rescaled inputs and outputs $\tilde{\mathcal{F}}_w$, which can be defined as

$$\mathcal{F}_w(\mathbf{P}) = \Psi_m^{-1} \mathbf{M}' = \Psi_m^{-1} [\tilde{\mathcal{F}}_w(\mathbf{P}')], \quad (2)$$

where \mathbf{M}' is the rescaled DNN approximation of the output.

B. Loss function

We want the DNN approximation to satisfy $\mathcal{F}_w(\mathbf{P}_i') \approx \mathbf{M}_i'$ for all $(\mathbf{P}_i', \mathbf{M}_i') \in S_t' \cup S_v'$. Therefore, we select the following loss function:

$$L(\tilde{\mathcal{F}}_w(\mathbf{P}_i'), \mathbf{M}_i') = \|\tilde{\mathcal{F}}_w(\mathbf{P}_i') - \mathbf{M}_i'\|_1, \quad (3)$$

where $\|\cdot\|_1$ is the l_1 norm.

C. Architecture

We use the architecture shown in Figure 2:

$$\tilde{\mathcal{F}}_w := \mathcal{L}_{w_N} \circ \mathcal{B}_{w_{N-1}}^{N-1} \circ \mathcal{B}_{w_{N-2}}^{N-2} \circ \dots \circ \mathcal{B}_{w_0}^0, \quad (4)$$

with $N = 5$. In the above, $w = \{w_i, i = 0, \dots, n\}$ are the weights (unknowns) of the DNN. Then, the blocks of the DNN are defined as:

$$\begin{aligned} \mathcal{B}_{w_i}^i &:= \left(\mathbf{n} \circ \mathbf{l}_{w_i^2}^c + \mathcal{I} \right) \left(\mathbf{n} \circ \mathbf{l}_{w_i^1}^c \right) \quad \forall i \in \{0, 1, \dots, 4\}, \\ \mathcal{L}_{w_5} &:= \left(\mathbf{n} \circ \mathbf{l}_{w_5^2}^d \circ \mathbf{R} \circ \mathbf{n} \circ \mathbf{l}_{w_5^1}^t \right), \end{aligned} \quad (5)$$

where $w_{(\cdot)} = \{w_{(\cdot)}^1, w_{(\cdot)}^2\}$ are the weights, \mathcal{I} is the identity operator, the functions \mathbf{l}^c , \mathbf{l}^d and \mathbf{l}^t represent a one-dimensional convolutional layer, a fully-connected layer, and a time-distributed layer, respectively. Furthermore, \mathbf{R} is a function that reshapes its input behind the last layer, and \mathbf{n} denotes the **activation function**. An activation function is a known simple non-linear function applied on its vector input component-wise, e.g., a sigmoid, or a rectified linear unit (ReLU). In this work, we consider the so called ReLU activation function:

$$\mathbf{n}(x_1, \dots, x_r) = (\max(0, x_1), \dots, \max(0, x_r)). \quad (6)$$

The described architecture gives a total of 462453 trainable parameters, also known as weights.

D. Training

We employ the training dataset to determine the weights w of Equation (4) by minimizing the cost function using the **ADAM** optimizer [37,]. Then, the validation dataset provides an initial assessment of the results, preventing unnoticed over-fitting, and enabling us to improve the architecture design. In the end, we analyze the final performance of our trained DNN using the test dataset.

After successful training of the DNN **offline**, the process of computing the forward function during real-time **online** operation reduces to evaluating a DNN. The online evaluation only requires a number of simple algebraic operations proportional to the number of weights and is computationally very fast.

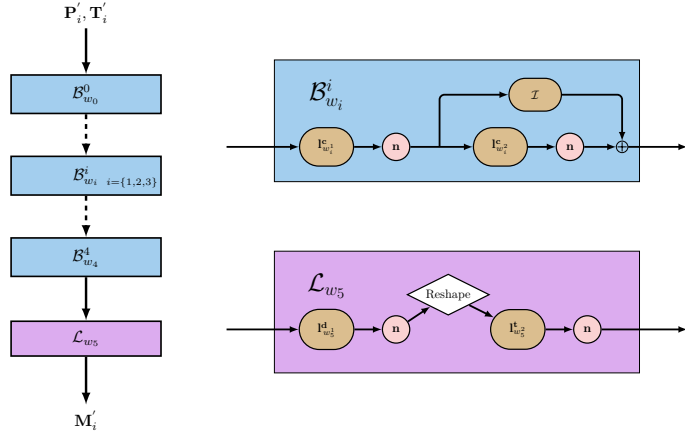


Fig. 2. Sketch of the DNN architecture and its blocks.

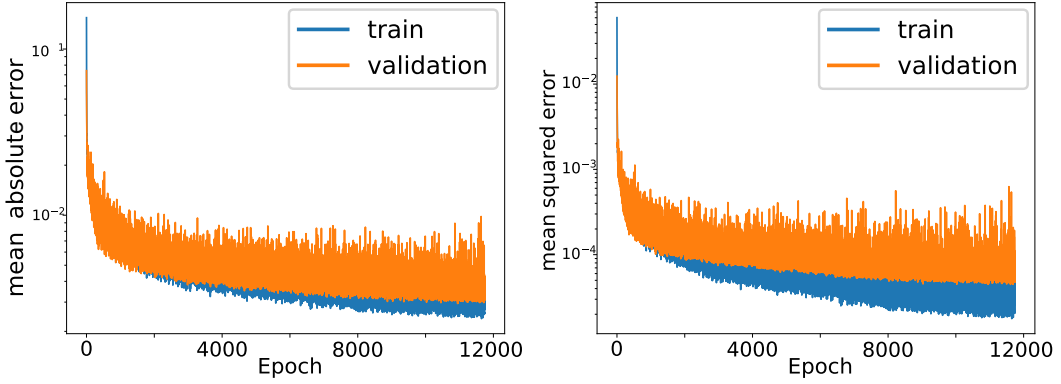


Fig. 3. History of decrease of mean absolute and mean squared error during training.

IV. NUMERICAL RESULTS

In this section we provide details on the training procedure and numerical verification of the methodology. First, we explain the details of the main training set-up and after that verify the accuracy on both the fit to the original dataset. Finally, we test the DNN-model on an independent example inspired by real geosteering operations in layer-cake geology. For that independent example we also compare the performance of another DNN-model trained on a smaller dataset \mathbf{D}^b .

A. Training

We train our DNN over multiple epochs on the training dataset from the *extended dataset* \mathbf{D}^e and batch size equal to 512. We use the default settings of the ADAM optimizer in Tensorflow [38,]. Then, we use the validation dataset for early stopping to prevent over-fitting utilizing the standard EarlyStopping callback in Tensorflow with patience (amount of epochs without decrease of the loss for validation dataset) set to 800. Figure 3 shows the reduction of training and validation errors. The early stopping was triggered after 11745 epochs with the total training phase taking around 13 hours on a consumer-grade GPU (RTX 2080ti). We use the weights obtained at epoch 10946 to produce the verification results in the rest of this section.

B. Cross-plots

While the training-validation datasets ensure that the model approximates the simulator reasonably well, they do not ensure that the model will generalize to other data points. Nor does the average error explain how well different measurements are reproduced.

In Figures 4-7 we present the data fit for all 13 real-time measurements discussed in Section II-B. The cross-plots show deviation of the predictions from the original high-fidelity forward model. The straight 45 degrees diagonal corresponds to the perfect fit. To give a numerical estimate of the quality of the fit we compute the coefficient of determination r^2 for each of measurements.

The fit of to the test data gives the r^2 coefficient of 0.99 and above demonstrating a well converged model. One can observe that classical shallow logs (Figure 4) give better data fit than deeper measurements. The deepest 20 kHz measurements (Figure

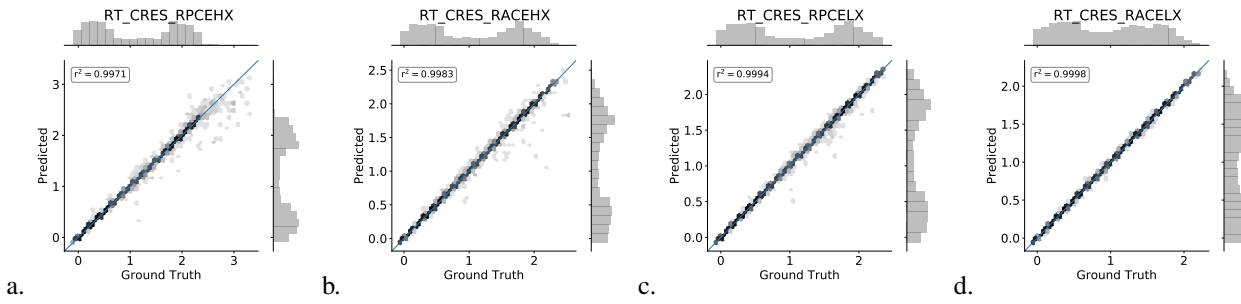


Fig. 4. Cross-plots of the predictions on test-data vs physical simulation for shallow resistivity logs. Resistivity estimated from phase difference (a) and attenuation (b) at 2 MHz frequency; phase difference (c) and attenuation (d) at 400 kHz frequency. Note the logarithmic scale.

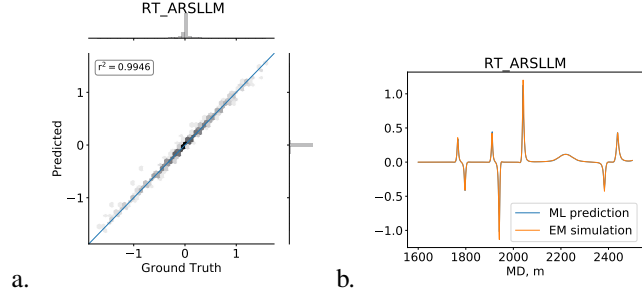


Fig. 5. a. Cross-plots of the predictions on test-data vs physical simulation for the 400 kHz imaginary measurement. b. A comparison of ML-based vs physical approximations of this log for the realistic test case in Figure 8. The measurements' scale has been normalized.

7) have a lower r^2 than the shallower 50 kHz analogs (Figure 6). This is intuitive since the approximation of the deeper measurements is more complex as it typically involves sensitivity to more layers.

C. Realistic example and discussion

To give an engineering insight into the quality of the model, in this section we generate a synthetic log for all measurements in a layer-cake environment for a near-horizontal well. The well trajectory and the horizontal layer-cake geomodel is presented in Figure 8. The log was sampled with a point each meter along the measured depth of the well, yielding a total of 901 logging positions.

This example represents a reasonably typical task for a predictive model in a real-time operation. Therefore it is important to verify the DNN's capability to provide quick and accurate results for such a setup.

The DNN is evaluated on a workstation running Intel Xeon(R) W-2155 CPU with 10 3.30GHz cores. For the full range of 901 logging positions along the well the evaluation takes 0.13 seconds, namely 0.15ms per logging position, which should suffice most of real-time needs for evaluation during inversion. The performance results are similar to those reported in [33,].

In Figures 9 through 11 and in 5b one can see the comparison between the logs predicted by the original physical simulation and by the trained DNN. All plots qualitatively coincide except some small inconsistencies near the boundaries between the layers.

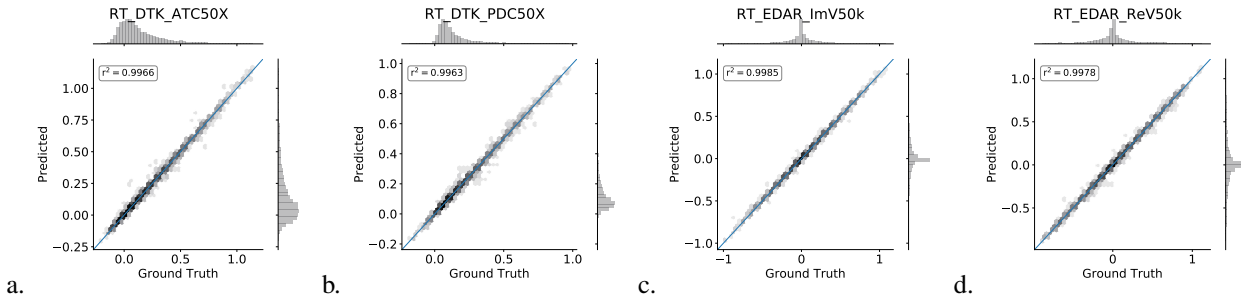


Fig. 6. Cross-plots of the predictions on test-data vs physical simulation for 50kHz measurements: attenuation (a) and phase (b) in dB; imaginary (c) and real (d) component in nV. The measurements' scales have been normalized to non-dimensional units.

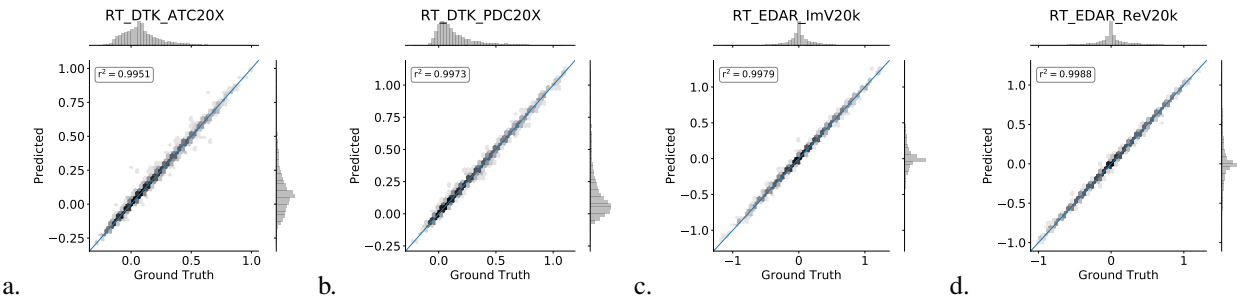


Fig. 7. Cross-plots of the predictions on test-data vs physical simulation for the deepest 20kHz measurements: attenuation (a) and phase (b) in dB; imaginary (c) and real (d) component in nV. The measurements' scales have been normalized to non-dimensional units.

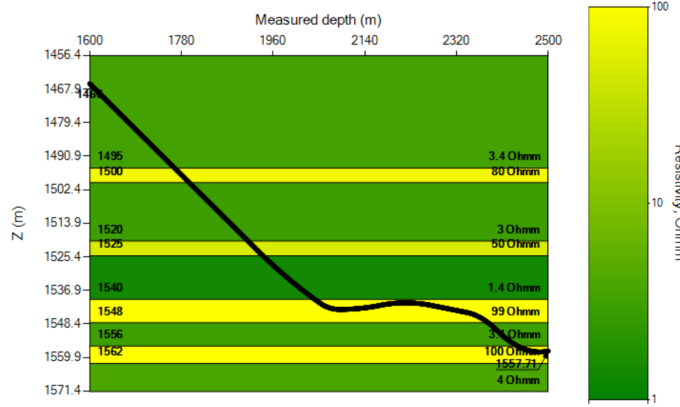


Fig. 8. The well trajectory and layer resistivities for the realistic log example in measured depth vs true vertical depth coordinates.

Since the example is generated separately from the training dataset it potentially contains combinations of values of angles, resistivities and depths which might have not been well captured in the training set. Specifically, the inconsistencies are pronounced before the landing in the reservoir for some of the deeper curves, see e.g. Figures 10a and 11a.

One reason is that there is an ambiguity of layer thicknesses when a degenerate model (which contains less layers) is converted to a 7-layer model during training and evaluation. Consequently, the measurements which have learned sensitivity to more layers are effected the most.

Another reason is that the training data contains a relatively low number of samples of this kind, see Section II-C. To that end, it is important to ensure that the model improves with the availability of relevant training data that better span the possible configurations.

Figures 10a and 11a additionally show the synthetic logs created by the same DNN architecture which was trained on the smaller *basic dataset D*^b which completely omits the 'semi-degenerate' samples which mimic the drilling in thick shales above reservoir, see Section II. The results in the initial 150 meters MD in these attenuation logs are clearly misrepresented by the DNN trained on a smaller dataset. We also observed the mismatch on other deep measurements, but it was less pronounced compared to the attenuation logs.

This indicates that the proposed architecture is suited for a larger range of realistic logging scenarios, and that the model quality will improve with additional data. At the same time, simply increasing the training dataset might be insufficient. We emphasize that to get high-quality data-driven approximations for this example we designed a dataset which captured the logging in thick shale layers.

V. CONCLUSIONS AND FURTHER WORK

In this work, we have demonstrated that a DNN can provide a high-quality approximation to a complex, industry-quality forward model for extra-deep EM logs used in modern geosteering operations. The DNN was trained using data generated with a numerical simulator provided by the logging instrument vendor but without access to or knowledge of its source code or the configuration of proprietary tools.

We considered a relatively small dataset of 63.122 samples to train a high-dimensional function $\mathcal{F}_w : \mathbb{R}^{22} \rightarrow \mathbb{R}^{13}$. By making the dataset geologically consistent and application-oriented, we were able to produce a good approximation to the relevant logs acquired during a synthetic geosteering operation. At the same time, our numerical examples show that the approximation works best within the regions which are best represented by the training data set. Therefore, extension of the dataset is required

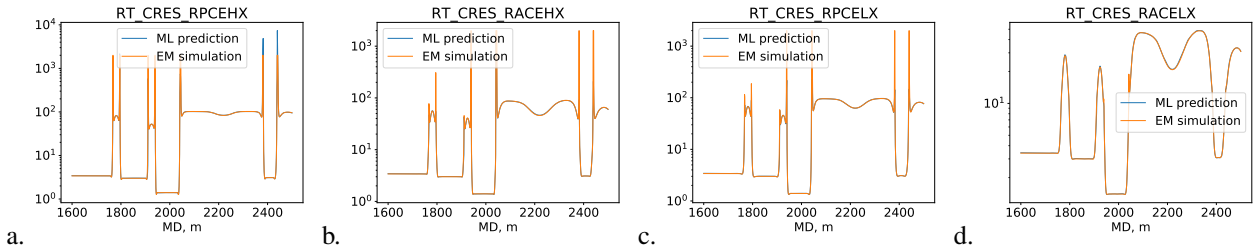


Fig. 9. A comparison of ML-based vs physical approximations for shallow resistivity logs on the realistic test from Figure 8. Resistivity estimated from phase difference (a) and attenuation (b) at 2 MHz frequency; phase difference (c) and attenuation (d) at 400 kHz frequency. Note the logarithmic scale.

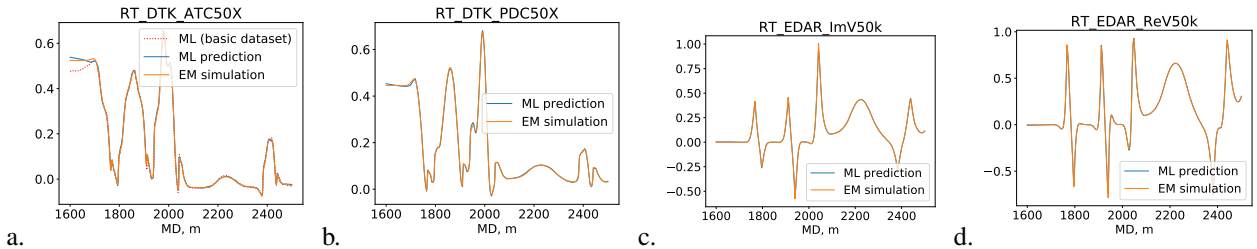


Fig. 10. A comparison of ML-based vs physical approximations for the 50 kHz measurements: attenuation (a) and phase (b) in dB; imaginary (c) and real (d) component in nV. The measurements' scales have been normalized to non-dimensional units.

when considering more scenarios, including lower angles typical for well landing, anisotropic resistivities, and more complex geological configurations.

We believe data-driven approximations as the one presented in this work are of crucial importance when it comes to future implementations of advanced inversion algorithms. Firstly, they become independent of the logging instrument vendor. Additionally, the resulting DNN forward model can be rapidly evaluated (in our work, it takes 0.15 milliseconds to evaluate all logs per logging position on a regular workstation). Such short execution times open the door for potential use as part of evaluation-hungry statistical and/or Monte-Carlo inversion algorithms.

REFERENCES

- [1] J. Seydoux, E. Legendre, E. Mirta, C. Dupuis, J.-M. Denichou, N. Bennett, G. Kutiev, M. Kuchenbecker, C. Morriss, and L. Y. Schlumberger, "Full 3D Deep Directional Resistivity Measurements Optimize Well Placement and Provide Reservoir-Scale Imaging While Drilling," in *SPWLA 55th Annual Logging Symposium*, 2014, p. 14.
- [2] C. Dupuis and V. Mendoza-Barron, "Avoid Pilot Holes, Land Wells, and Optimize Well Placement and Production with Deep Directional Resistivity Logging-While-Drilling," *SPE Bergen One Day Seminar*, pp. 1–8, 2014. [Online]. Available: <http://www.onepetro.org/doi/10.2118/169206-MS>
- [3] D. Larsen, Y. Antonov, P. Luxey, J. Skillings, M. B. Skaug, V. Wagner *et al.*, "Navigating the horizontal section in a heterogeneous formation while using extra deep azimuthal resistivity for optimizing the wellbore placement within a narrow tvt window," in *SPWLA 57th Annual Logging Symposium*. Society of Petrophysicists and Well-Log Analysts, 2016.
- [4] M. Shahriari and D. Pardo, "Borehole resistivity simulations of oil-water transition zones with a 1.5D numerical solver," *Computational Geosciences*, 2020.
- [5] H.-H. M. Wu, L. Pan, J. Ma, W. Dong, Y. Fan, C. Lozinsky, M. Bittar *et al.*, "Enhanced reservoir geosteering and geomapping from refined models of ultra-deep lwd resistivity inversions using machine-learning algorithms," in *SPWLA 60th Annual Logging Symposium*. Society of Petrophysicists and Well-Log Analysts, 2019.
- [6] D. S. Larsen, D. Boesing, A. Hartmann, S. Martakov, A. Mumtaz, and J. Skillings, "Boundary Detection Ahead of the Bit A Sensitivity Study of Extra Deep Azimuthal Resistivity," in *Offshore Technology Conference Asia held in Kuala Lumpur, Malaysia*, 2018.
- [7] M. Shahriari, S. Rojas, D. Pardo, A. Rodríguez-Rozas, S. A. Bakr, V. M. Calo, and I. Muga, "A numerical 1.5D method for the rapid simulation of geophysical resistivity measurements," *Geosciences*, vol. 8(6), pp. 1–28, 2018.

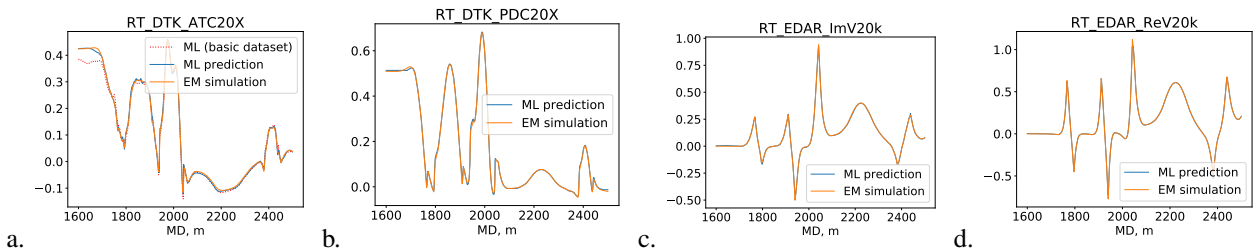


Fig. 11. A comparison of ML-based vs physical approximations for the 20 kHz measurements: attenuation (a) and phase (b) in dB; imaginary (c) and real (d) component in nV. The measurements' scales have been normalized to non-dimensional units.

- [8] S. Davydcheva, M. Zhou, and R. Liu, "Triaxial induction tool response in 1d layered biaxial anisotropic formation," in *SEG Technical Program Expanded Abstracts 2014*. Society of Exploration Geophysicists, 2014, pp. 643–648.
- [9] S. Alyaev, E. Suter, R. B. Bratvold, A. Hong, X. Luo, and K. Fossum, "A decision support system for multi-target geosteering," *Journal of Petroleum Science and Engineering*, vol. 183, p. 106381, dec 2019. [Online]. Available: <https://linkinghub.elsevier.com/retrieve/pii/S0920410519308022>
- [10] X. Luo, P. Eliasson, S. Alyaev, A. Romdhane, E. Suter, E. Querendez, and E. Vefring, "An ensemble-based framework for proactive geosteering," in *SPWLA 56th Annual Logging Symposium, July 18-22, 2015*, 2015, pp. 1–14.
- [11] T. Deng, J. Ambía, C. Torres-Verdín *et al.*, "Fast bayesian inversion method for the generalized petrophysical and compositional interpretation of multiple well logs with uncertainty quantification," in *SPWLA 60th Annual Logging Symposium*. Society of Petrophysicists and Well-Log Analysts, 2019.
- [12] H. V. Le, S. Mayer, and N. Henze, "Machine learning with tensorflow for mobile and ubiquitous interaction," in *Proceedings of the 16th International Conference on Mobile and Ubiquitous Multimedia*, ser. MUM 17. New York, NY, USA: Association for Computing Machinery, 2017, p. 567572. [Online]. Available: <https://doi.org/10.1145/3152832.3156559>
- [13] C. Higham and D. Higham, "Deep learning: An introduction for applied mathematicians," *Computing Research Repository*, vol. abs/1801.05894, 2018.
- [14] K. He, X. Zhang, S. Ren, and J. Sun, "Deep residual learning for image recognition," *arXiv:1512.03385*, 2015.
- [15] B. Bhanu and A. Kumar, *Deep Learning for Biometrics*. Springer, Switzerland, 2017.
- [16] L. Lu, Y. Zheng, G. Carneiro, and L. Yang, *Deep Learning for Computer Vision: Expert techniques to train advanced neural networks using TensorFlow and Keras*. Springer, Switzerland, 2017.
- [17] D. Yu and L. Deng, *Automatic Speech Recognition: A Deep Learning approach*. Springer, London, 2017.
- [18] B. B. Boughei, "Machine learning applications to geophysical data analysis," Master's thesis, The University of British Columbia, 2016.
- [19] M. Araya-Polo, T. Dahlke, C. Frogner, C. Zhang, T. Poggio, and D. Hohl, "Automated fault detection without seismic processing," *Leading Edge*, vol. 36, no. 3, pp. 208–214, 2017.
- [20] D. J. Lary, A. H. Alavi, A. H. Gandomi, and A. L. Walker, "Machine learning in geosciences and remote sensing," *Geoscience Frontiers*, vol. 7, no. 1, pp. 3–10, 2016, special Issue: Progress of Machine Learning in Geosciences.
- [21] C. Hegde, S. Wallace, and K. Gray, "Using trees, bagging, and random forests to predict rate of penetration during drilling," *Society of Petroleum Engineers*, pp. 1–12, 2015.
- [22] A. Aulia, A. Rahman, and J. J. Q. Velasco, "Strategic well test planning using random forest," *Society of Petroleum Engineers*, pp. 1–23, 2014.
- [23] N. Bize-Forest, L. Lima, V. Baines, A. Boyd, F. Abbotts, and A. Barnett, "Using machine-learning for depositional facies prediction in a complex carbonate reservoir," *Society of Petrophysicists and Well-Log Analysts*, pp. 1–11, 2018.
- [24] V. Puzyrev, "Deep learning electromagnetic inversion with convolutional neural networks," *Geophysical Journal International*, vol. 218, no. 2, pp. 817–832, 05 2019. [Online]. Available: <https://doi.org/10.1093/gji/ggz204>
- [25] Y. Ge, W. Wu, R. Wang, L. He *et al.*, "Porosity evaluation of igneous rocks based on deep learning," in *SEG International Exposition and Annual Meeting*. Society of Exploration Geophysicists, 2019.
- [26] D. Moghadas, "One-dimensional deep learning inversion of electromagnetic induction data using convolutional neural network," *Geophysical Journal International*, vol. 222, no. 1, pp. 247–259, 04 2020. [Online]. Available: <https://doi.org/10.1093/gji/ggaa161>
- [27] Y. Chen and D. Zhang, "Physics-constrained deep learning of geomechanical logs," *IEEE Transactions on Geoscience and Remote Sensing*, 2020.
- [28] D. Colombo, W. Li, E. Sandoval-Curiel, and G. W. McNeice, "Deep-learning electromagnetic monitoring coupled to fluid flow simulators," *Geophysics*, 2020.
- [29] J. He and S. Misra, "Generation of synthetic dielectric dispersion logs in organic-rich shale formations using neural-network models," *Geophysics*, vol. 84, no. 3, pp. D117–D129, 2019.
- [30] G. Zhu, M. Gao, F. Kong, and K. Li, "A fast inversion of induction logging data in anisotropic formation based on deep learning," *IEEE Geoscience and Remote Sensing Letters*, pp. 1–5, 2020.
- [31] M. Shahriari, D. Pardo, A. Picón, A. Galdran, J. D. Ser, and C. Torres-Verdín, "A deep learning approach to the inversion of borehole resistivity measurements," *Computational Geosciences*, 2020. [Online]. Available: <https://doi.org/10.1007/s10596-019-09859-y>
- [32] M. Shahriari, D. Pardo, B. Moser, and F. Sobieczky, "A deep neural network as surrogate model for forward simulation of borehole resistivity measurements," *Procedia Manufacturing*, vol. 42, pp. 235 – 238, 2020, international Conference on Industry 4.0 and Smart Manufacturing (ISM 2019).
- [33] D. Kushnir, N. Velker, A. Bondarenko, G. Dyatlov, and Y. Dashevsky, "Real-Time Simulation of Deep Azimuthal Resistivity Tool in 2D Fault Model Using Neural Networks," *Society of Petroleum Engineers*, 2018.
- [34] M. Sviridov, A. Mosin, Y. Antonov, M. Nikitenko, S. Martakov, M. B. Rabinovich, Baker Hughes, and BP, "New Software for Processing of LWD Extradep Resistivity and Azimuthal Resistivity Data," *Spe Reservoir Evaluation & Engineering*, vol. 17, no. May, pp. 109–127, 2014.
- [35] A. Hartmann, A. Vianna, H.-m. Maurer, M. Sviridov, S. Martakov, B. Hughes, F. Antonsen, P. A. Olsen, and M. V. Constable, "Verification Testing of a New Extra-Deep Azimuthal Resistivity Measurement," in *SPWLA 55th annual logging symposium*. SPWLA, 2014, pp. 1–12.
- [36] J. Bennett, "Autoit scripting language," 1999, accessed: 2020-04-24. [Online]. Available: <https://www.autoitscript.com/>
- [37] D. P. Kingma and J. Ba, "Adam: A method for stochastic optimization," 2014.
- [38] M. Abadi, A. Agarwal, P. Barham, E. Brevdo, Z. Chen, C. Citro, G. S. Corrado, A. Davis, J. Dean, M. Devin, S. Ghemawat, I. Goodfellow, A. Harp, G. Irving, M. Isard, Y. Jia, R. Jozefowicz, L. Kaiser, M. Kudlur, J. Levenberg, D. Mané, R. Monga, S. Moore, D. Murray, C. Olah, M. Schuster, J. Shlens, B. Steiner, I. Sutskever, K. Talwar, P. Tucker, V. Vanhoucke, V. Vasudevan, F. Viégas, O. Vinyals, P. Warden, M. Wattenberg, M. Wicke, Y. Yu, and X. Zheng, "TensorFlow: Large-scale machine learning on heterogeneous systems," 2015, software available from tensorflow.org. [Online]. Available: <http://tensorflow.org/>



Sergey Alyaev is a senior researcher in applied mathematics at NORCE with interests including forward and inverse modeling, data-driven methods, and decision theory. Sergey has MSc and PhD degrees in applied mathematics from the University of Bergen. The main focuses of his research are the real-time applications of these methods and integrated workflows in the field of drilling and geosteering. From 2018 he took responsibility for leading the project Geosteering for IOR where the team is developing advanced quantitative and statistical methods and applying them for real-time decision making.



Mostafa Shahriari holds a PhD degree in computational mathematics from the university of the Basque Country (UPV/EHU). In 2018, he became a postdoctoral fellow at BCAM and then at Euskampus. He is currently a researcher in Software Competence Center Hagenberg (SCCH) in Austria. His main research interest focus on the application of advanced Artificial Intelligence (AI) algorithms for computational engineering.



David Pardo is a Research Professor at Ikerbasque, the University of the Basque Country UPV/EHU, and the Basque Center for Applied Mathematics (BCAM). He has published over 160 research articles and he has given over 260 presentations. In 2011, he was awarded as the best Spanish young researcher in Applied Mathematics by the Spanish Society of Applied Mathematics (SEMA). He leads a European Project on subsurface visualization, several national research projects, as well as research contracts with national and international companies. He is now the PI of the research group on Applied Mathematical Modeling, Statistics, and Optimization (MATHMODE). His research interests include computational electromagnetics, petroleum-engineering applications (borehole simulations), adaptive finite-element and discontinuous Petrov-Galerkin methods, multigrid solvers, deep learning algorithms, and multiphysics and inverse problems.



Àngel J. Omella received his PhD degree in computational mechanics from the University of Zaragoza (Spain) in 2017. From 2017 to 2019, he was a Postdoctoral Fellow in Computational and Applied Mathematics at the Basque Center for Applied Mathematics (BCAM). In 2019, he moved to the Department of Applied Mathematics, Statistics and Operations Research at the University of the Basque Country (UPV/EHU). His research interests include solving inverse problems, finite-element methods, and regression methods based on neural networks.



David Selvåg Larsen is currently working as the Digitalization Manager in Europe for Baker Hughes. He recently came from the Global R&D Technical Lead position within BKR and has more than 8 years of geosteering experience. David started working for Baker Hughes Norge in 2010 and holds a M.Sc. in Marine Geophysics from the Univ. of Tromsø, Norway.



Nazanin Jahani received her PhD degree in mechanical engineering from the Norwegian University of Science and Technology (NTNU) in Trondheim in 2015. She is currently a researcher at the energy department of NORCE Norwegian Research centre. Her research interests include computational physics in petroleum applications. Since 2018, she is a project member for the project Geosteering for IOR, working on forward-modelling tools to estimate formation properties as input parameters for real-time decision making.



Erich Suter is a Postdoctoral Scientist at NORCE (Norwegian Research Centre) in Stavanger. He holds a PhD degree in Computational Geoscience from the University of Stavanger, an MSc degree in Applied Mathematics (geometric modelling) from the University of Oslo and a BSc degree in Information Technology from Gjvik University College (now NTNU). His research interests are within effective geological interpretation and earth model management for real-time applications, e.g. decision support under uncertainty while geosteering and reservoir model construction/updating. He is skilled within applied mathematics and computer science, petroleum geology, geometric modelling and software design and development.